

Dynamical heterogeneity in periodically deformed polymer glasses

Nikolai V. Priezjev

Department of Mechanical and Materials Engineering,

Wright State University, Dayton, OH 45435

(Dated: March 22, 2021)

Abstract

The dynamics of structural relaxation in a model polymer glass subject to spatially-homogeneous, time-periodic shear deformation is investigated using molecular dynamics simulations. We study a coarse-grained bead-spring model of short polymer chains below the glass transition temperature. It is found that at small strain amplitudes, the segmental dynamics is nearly reversible over about 10^4 cycles, while at strain amplitudes above a few percent, polymer chains become fully relaxed after a hundred cycles. At the critical strain amplitude, the transition from slow to fast relaxation dynamics is associated with the largest number of dynamically correlated monomers as indicated by the peak value of the dynamical susceptibility. The analysis of individual monomer trajectories showed that mobile monomers tend to assist their neighbors to become mobile and aggregate into relatively compact transient clusters.

PACS numbers: 61.43.Fs, 61.43.-j, 64.70.pj, 83.10.Rs

I. INTRODUCTION

The analysis and optimization of the mechanical performance of amorphous polymers are critical for various industrial and biomedical applications [1]. In the absence of external deformation, the molecular motion slows down and a polymer glass gradually evolves towards an equilibrium state in a process called *physical aging*, which affects mechanical properties of the material [2]. In turn, the effects of physical aging can be removed by application of mechanical stresses or by heating above the glass transition temperature and then cooling back down [2]. According to the well-known Eyring model, an applied stress lowers the effective energy barriers for molecular motion and thus induces yield and plastic flow in polymer glasses [3]. This simple description, however, does not include the effects of dynamical heterogeneity, strain localization, and strain hardening [4, 5].

It was previously demonstrated that the relaxation dynamics in *quiescent* polymer glasses near the glass transition temperature becomes spatially heterogeneous [6–8]. In particular, it was shown that the most mobile monomers form transient clusters whose mean size increases upon cooling towards the glass transition temperature [7]. In some cases, neighboring monomers undergo large displacements and follow each other in a string-like fashion [8]. Near T_g , the average string length was found to be about two monomer diameters, although strings of about ten monomers were observed [8]. As expected, polymer chain ends are more mobile; however, the mobility does not necessarily propagate along the backbone of the chains [8]. More recently, the spatiotemporal distribution of monomer hopping events was investigated in an aging polymer glass quenched below the glass transition temperature [9]. It was shown that before merging into a single dominating cluster, the volume distribution of clusters of hopping monomers follows a power-law decay with an exponent of two, and the clusters have slightly noncompact shapes [9].

The segmental mobility during *constant stress or strain rate deformation* of polymer glasses was recently studied experimentally [10–12] and using molecular dynamics (MD) simulations [13–18]. In general, it was shown that after flow onset, the segmental mobility is strongly accelerated and the distribution of relaxation times is narrowed under active deformation. It was also found that before the onset of flow, the deformation-induced molecular mobility is spatially heterogeneous, involving the formation of clusters of mobile molecules [16]. By decomposing monomer trajectories into a series of rapid hopping events,

it was observed that the distribution of the first hop and persistence times is narrowed, which indicates that the monomer relaxation dynamics is accelerated during constant strain rate deformation [17, 18]. As a complimentary approach to probe glassy dynamics, the analysis of individual particle trajectories was also performed in amorphous materials under *cyclic shear deformation* [19–25]. By employing a novel cage decomposition algorithm, it was demonstrated that intermittent bursts of cage jumps are directly correlated with the major structural relaxation events in a two-dimensional dense granular media [19]. It was further pointed out that the relaxation process involves spatially clustered cage jumps, which on long time scales aggregate into avalanches [19].

In a recent study [21], the relaxation dynamics in periodically deformed binary Lennard-Jones mixture was examined at a finite temperature well below the glass transition. It was found that the mean-square displacement develops an extended subdiffusive plateau associated with cage-trapping, and the particle dynamics becomes spatially and temporally heterogeneous. Furthermore, the dynamic correlation length, which was estimated from the peak of the dynamical susceptibility, grows with increasing strain amplitude up to a value that corresponds to the largest size of dynamically correlated regions. One of the aims of the current study is to test whether these conclusions hold for nonentangled polymer glasses under cyclic loading.

In this paper, we investigate structural relaxation and dynamical heterogeneity in a bead-spring model of low-molecular-weight polymer glass that is subject to spatially homogeneous, time-periodic shear deformation. We find that at sufficiently small strain amplitudes, the system dynamics is nearly reversible, while at amplitudes above a few percent, monomers undergo irreversible cage jumps that become spatially aggregated into relatively compact clusters. It will be shown that at the critical strain amplitude, the dynamic correlation length exhibits a distinct maximum indicating the largest size of regions over which the motion of monomers is spatially correlated.

The rest of the paper is structured as follows. The description of molecular dynamics simulations is presented in Sec. II. In Sec. III, we examine the mean-square displacement of monomers, the autocorrelation function of normal modes, as well as the self-correlation function and dynamical susceptibility, followed by the analysis of the monomer hopping dynamics and the discussion of dynamic facilitation. Brief conclusions are provided in the final section.

II. DETAILS OF MOLECULAR DYNAMICS SIMULATIONS

In this study, we perform molecular dynamics simulations of the coarse-grained bead-spring model of flexible polymer chains [26]. The system consists of 312 linear chains of $N = 10$ monomers each confined in a periodic cubic cell. A snapshot of the polymer glass at zero strain is shown in Fig. 1. The pairwise interaction between monomers is specified by the truncated Lennard-Jones (LJ) potential

$$V_{LJ}(r) = 4 \varepsilon \left[\left(\frac{\sigma}{r} \right)^{12} - \left(\frac{\sigma}{r} \right)^6 \right], \quad (1)$$

where the parameters ε and σ denote the energy and length scales, respectively. The cutoff radius is fixed to $r_c = 2.245 \sigma$. The total number of monomers in the system is $N_m = 3120$. In addition to the LJ potential, any two neighboring beads in a polymer chain interact via the finitely extensible nonlinear elastic (FENE) potential [27]

$$V_{FENE}(r) = -\frac{k_s}{2} r_o^2 \ln[1 - r^2/r_o^2], \quad (2)$$

with the parameters $k_s = 30 \varepsilon \sigma^{-2}$ and $r_o = 1.5 \sigma$ [26]. The effective bond potential between neighboring beads does not allow chain crossings and bond breaking even at the highest strain amplitude considered in the present study.

The simulations were carried out at a constant temperature of $0.1 \varepsilon/k_B$, which is below the glass transition temperature $T_g \approx 0.32 \varepsilon/k_B$ [28]. Here, k_B is the Boltzmann constant. To keep the system temperature at $0.1 \varepsilon/k_B$, the velocity component perpendicular to the plane of deformation was rescaled every 10 MD steps. The polymer glass was confined into a cubic box with a side length of 14.29σ , resulting in a monomer density $\rho = 1.07 \sigma^{-3}$ (see Fig. 1). A homogeneous shear deformation was imposed using the SLLOD algorithm combined with the Lees-Edwards periodic boundary conditions [29]. The equations of motion were integrated using the fifth-order Gear predictor-corrector algorithm [30] with a time step $\Delta t_{MD} = 0.005 \tau$, where $\tau = \sigma \sqrt{m/\varepsilon}$ is the LJ time.

After equilibration for about 5×10^6 MD steps, the cyclic shear strain was applied in the xz plane by varying strain as a function of time as follows

$$\gamma(t) = \gamma_0 \sin(\omega t), \quad (3)$$

where γ_0 is the strain amplitude and ω is the oscillation frequency. In our simulations, the oscillation frequency and period were fixed to $\omega \tau = 0.05$ and $T = 2\pi/\omega = 125.66 \tau$,

respectively. The maximum strain amplitude considered in the present study, $\gamma_0 = 0.09$, is greater than the yield strain. After discarding transients, the positions of all monomers were saved every back and forth cycle when the net strain is zero, and the data were gathered over 15 000 cycles (about 3.8×10^8 MD steps) at each strain amplitude. Therefore, as the cyclic loading continues, the structural changes in the material are related to the degree of overlap between monomer configurations at different times. The post-processing analysis of the MD data was carried out in ten independent samples for each γ_0 .

III. RESULTS

The molecular structure of amorphous polymers is characterized by the short-range order and the absence of any long-range order or symmetry [31]. During the time-periodic, steady-state deformation, monomers of a polymer chain either remain trapped within cages formed by their neighbors or undergo irreversible displacements, which gives rise to a diffusion process. Figure 2 shows the time dependence of the mean-square displacement of monomers for different strain amplitudes. Before averaging, the displacement vector for each monomer was computed with respect to the center of mass of the whole system. It can be seen that with increasing strain amplitude, the characteristic time for the onset of the diffusive motion decreases. Notice that at small strain amplitudes, $\gamma_0 = 0.02$ and 0.03 , monomers remain trapped in their cages during the time interval $15\,000 T$, while at larger amplitudes, $\gamma_0 = 0.04$ and 0.05 , monomers escape from their cages after about $1000 T$. When $\gamma_0 \geq 0.06$, the monomer dynamics is slightly subdiffusive at long times as the displacement of monomers is restricted by the motion of the center of mass of polymer chains. Interestingly, at large strain amplitudes $\gamma_0 \geq 0.07$, monomers, on average, move out from their cages during a single oscillation cycle. Lastly, the ballistic regime occurs at shorter time scales than the oscillation period $T = 125.66 \tau$, and, therefore, it is not present in any of the curves in Fig. 2.

The relaxation dynamics of polymer chains can be probed by analyzing the decay of the time autocorrelation function of normal modes [32, 33]. For a polymer chain that consists of N monomers, the normal coordinates are defined by

$$\mathbf{X}_p(t) = \frac{1}{N} \sum_{i=1}^N \mathbf{r}_i(t) \cos \frac{p\pi(i-1/2)}{N}, \quad (4)$$

where \mathbf{r}_i is the position vector of the i -th monomer and $p = 0, 1, \dots, N-1$ is the mode

number. The shortest and longest relaxation times correspond to the last $p = N - 1$ and the first $p = 1$ modes. Correspondingly, the time autocorrelation function for the p -th normal mode is computed as follows:

$$C_p(t) = \langle \mathbf{X}_p(t) \cdot \mathbf{X}_p(0) \rangle / \langle \mathbf{X}_p(0) \cdot \mathbf{X}_p(0) \rangle, \quad (5)$$

where the angle brackets denote averaging over initial times and independent samples. The time dependence of the correlation functions $C_1(t)$ and $C_9(t)$ is presented in Fig. 3 for the oscillation frequency $\omega\tau = 0.05$ and different strain amplitudes. The orientational dynamics of the whole chain is described by the function $C_1(t)$. It is evident from Fig. 3 (a), that the orientation of polymer chains is unaffected by the periodic deformation for strain amplitudes $\gamma_0 \leq 0.05$, while they become fully relaxed for $\gamma_0 \geq 0.07$ during the reported time interval. As expected, the segmental dynamics is faster; e.g., the function $C_9(t)$ decays to nearly zero after 1.5×10^4 cycles for the strain amplitude $\gamma_0 = 0.06$, as shown in Fig. 3 (b). These results indicate that with increasing amplitude of the shear strain deformation, the relaxation dynamics of polymer chains undergoes a transition at the strain amplitude of about $\gamma_0 \approx 0.06$.

The structural relaxation process in glassy materials often involves spatial fluctuations of particle mobilities [34]. During periodic deformation, the degree of overlap between two spatial configurations of monomers is described by the self-correlation function, which is defined as follows:

$$Q_s(a, t) = \frac{1}{N_m} \sum_{i=1}^{N_m} \exp\left(-\frac{\Delta \mathbf{r}_i(t)^2}{2a^2}\right), \quad (6)$$

where $\Delta \mathbf{r}_i(t) = \mathbf{r}_i(t_0 + t) - \mathbf{r}_i(t_0)$ is the displacement vector of the i -th monomer during the time interval t , N_m is the total number of monomers, and a is the probed length scale [35]. Furthermore, it was previously shown that the dynamical heterogeneity can be quantified via the variance of the self-correlation function, or the dynamical susceptibility, which is given by

$$\chi_4(a, t) = N_m [\langle Q_s(a, t)^2 \rangle - \langle Q_s(a, t) \rangle^2], \quad (7)$$

where the averaging is performed over all initial times [36]. An example of the correlation functions $Q_s(a, t)$ and $\chi_4(a, t)$ is presented in Fig. 4 for the strain amplitude $\gamma_0 = 0.06$. The contour plots clearly show that during the reported time interval the structural relaxation occurs on the length scale of about the cage size, and the dynamical susceptibility $\chi_4(a, t)$ reaches a maximum at intermediate length and time scales, thus providing an estimate for a number of monomers involved in a correlated motion.

To gain further insight into the relaxation process, we fix the probed length scale to a value slightly larger than the cage size, i.e., $a = 0.12\sigma$, and plot the self-correlation function $Q_s(a, t)$ versus time in Fig. 5 for different strain amplitudes. It is clearly observed that the structural relaxation occurs faster at larger strain amplitudes. In particular, at small strain amplitudes, $\gamma_0 \leq 0.02$, the monomers remain trapped inside their cages, indicating that the system dynamics is nearly reversible during the reported time interval; while for $\gamma_0 \geq 0.07$, the system becomes fully relaxed after about 100 cycles. Similar to the behavior of the autocorrelation function of normal modes shown in Fig. 3, the transition from slow to fast dynamics occurs at the same strain amplitude $\gamma_0 \approx 0.06$. Also, the results in Fig. 5 are consistent with the time dependence of the mean-square displacement curves reported in Fig. 2.

While analyzing the dynamical susceptibility at different strain amplitudes, we found that for each γ_0 the location of the maximum of $\chi_4(a, t)$ depends both on a and t . In Fig. 6, the dynamical susceptibility is shown as function of time for the values of the parameter a at which $\chi_4(a, t)$ has a global maximum at a given strain amplitude. It is apparent that with increasing strain amplitude, the position of the peak in $\chi_4(a, t)$ is shifted to smaller times. The amplitude of the peak, which reflects the typical number of monomers involved in a correlated motion, has a pronounced maximum at the strain amplitude $\gamma_0 = 0.06$. Notice also that at larger strain amplitudes, $\gamma_0 = 0.08$ and 0.09 , the maximum of $\chi_4(a, t)$ occurs after the first cycle.

Assuming that correlated regions are relatively compact, the dynamic correlation length ξ_4 can be simply estimated from the peak value of the dynamical susceptibility, i.e., $\xi_4 = [\chi_4^{\max}(a, t)]^{1/3}$. Taking the maximum of the curves in Fig. 6, the variation of the correlation length ξ_4 as a function of the strain amplitude is presented in the inset of Fig. 6. Interestingly, the correlation length exhibits a distinct maximum at the critical strain amplitude $\gamma_0 = 0.06$. These results reveal that the transition from slow to fast relaxation dynamics reported in Figs. 2, 3, and 5 is accompanied by the largest number of dynamically correlated monomers.

We emphasize that a qualitatively similar behavior of the dynamic correlation length was observed in the previous study on cyclic deformation of a binary Lennard-Jones glass [21]. In that study, however, the maximum of the dynamical susceptibility $\chi_4(a, t)$ was computed at the same value of the parameter $a = 0.12\sigma$ for all strain amplitudes, and the estimate of the dynamic correlation length was reported up to a strain amplitude at which the number of

particles involved in a correlated motion is maximum [21]. In general, the initial growth of the dynamic correlation length with increasing strain amplitude during oscillatory deformation is in marked contrast to the situation in glassy materials under steady shear, where the relaxation dynamics becomes more homogeneous with increasing shear rate [37, 38]. On the other hand, our results are consistent with the conclusions of the previous study by Riggleman *et al.* [16], who found that at a constant strain rate deformation of polymer glasses, the relaxation dynamics is strongly heterogeneous below the yield strain, and after the onset of flow, the dynamics becomes significantly more homogeneous.

We now turn to a discussion of the monomer hopping dynamics and the formation of transient clusters of mobile monomers. Under cyclic loading, the motion of a monomer involves thermal vibration within the cage formed by its neighbors and rapid hopping from one cage to another. The cage jumps can be identified by a numerical algorithm that was originally introduced by Candelier *et al.* [19]. This method, called the *iterative barycenters separation*, computes the effective distance between two consecutive segments of a monomer trajectory. If this distance is larger than the typical cage size then the trajectory is divided into two subsets. Using the iterative procedure, the trajectory of each monomer can be decomposed into consecutive segments where the displacement of a monomer is localized within cages formed by its neighbors [19]. This algorithm was used to locate cage jumps in two-dimensional granular systems [19, 39] and supercooled liquids [40]. More recently, the cage decomposition algorithm was implemented to identify cage jumps ‘on-the-fly’ during the simulation run, thus eliminating the need to store multiple particle configurations [9].

In this work, the monomer trajectories were stored and analyzed following the cage decomposition method proposed by Candelier *et al.* [19]. Similar to the implementation of the algorithm used in our previous study [21], we first take a part of the monomer trajectory, cut it in two adjacent segments, and then compute the effective distance between them. If this distance is less than the cage size, $r_c = 0.1 \sigma$, for any two adjacent segments within the sub-trajectory, then we conclude that the monomer remained within the cage. Using this brute-force procedure, we examined all time intervals $10 T \leq \Delta t_a \leq 100 T$ for all monomer trajectories. We found that cage jumps typically occur during several cycles, and they can be either reversible, when a monomer jumps back to its previous cage, or irreversible otherwise.

The total number of mobile monomers is plotted as a function of time in Fig. 7 for the strain amplitudes $\gamma_0 = 0.02, 0.04, \text{ and } 0.06$. As is evident, in each case the relaxation

dynamics is characterized by sudden bursts in mobility separated by periods of quiescence. Note that at the strain amplitude $\gamma_0 = 0.02$, mobile monomers mostly undergo reversible jumps without any net displacement (see Fig. 2), while at $\gamma_0 = 0.06$, the amplitude of bursts is about half of the total number of monomers in the system. Moreover, a visual inspection of snapshots indicates that mobile monomers tend to form clusters. Examples of instantaneous monomer positions during intermittent bursts are shown in Fig. 8 for different strain amplitudes. It can be seen that the clusters have a relatively compact structure, although several monomers appear to be isolated. Notice the formation of a large cluster at $\gamma_0 = 0.06$ that spans the whole system. As the cyclic deformation continues, the number of mobile monomers in a large cluster decreases typically to a few monomers that undergo reversible jumps until the emergence of the next cluster. Thus, the spatio-temporal clusterization algorithm [19] would identify only several large-size clusters, rendering their statistics unreliable.

A number of previous studies have explored the effect of dynamic facilitation in glassy materials and concluded that a particle has a higher probability to become mobile if it has a neighboring particle that was previously mobile [21, 39, 41, 42]. Here, we analyzed a trajectory of each monomer, using the cage decomposition algorithm described above, and identified cage jumps and time intervals when a monomer remained within the cage. If a monomer escaped its cage and had at least one nearest-neighbor that was mobile sometime during the time interval Δt preceding the cage jump, then this hop event was considered to be facilitated by the neighbors. The ratio of dynamically facilitated mobile monomers and the total number of mobile monomers is plotted in Fig. 9 as a function of the time interval preceding cage jumps. It can be observed that the ratio N_f/N_{tot} increases rapidly and appears to saturate after about 2000 cycles. With increasing strain amplitude, the fraction of dynamically facilitated mobile monomers increases. It is perhaps not surprising that the ratio is nearly one for $\gamma_0 = 0.06$ because most of the monomers undergo cage jumps during the time interval $10^4 T$ and thus influence hopping of their neighbors. The fact that the ratio is about 0.6 for the strain amplitude $\gamma_0 = 0.02$, at which the self-correlation function remains nearly constant (see Fig. 5), suggests that reversible cage jumps are either spatially isolated or clustered in small groups at the same locations during the reported time interval.

IV. CONCLUSIONS

In summary, molecular dynamics simulations were carried out to investigate structural relaxation and dynamical heterogeneity in a model polymer glass under oscillatory shear strain. We used a standard bead-spring representation of linear polymer chains below the entanglement regime. To probe the microscopic relaxation dynamics, we examined the mean-square displacement of monomers, the autocorrelation function of normal modes, as well as the self-overlap order parameter and dynamical susceptibility.

It was found that the segmental mobility is unaffected by the time-periodic deformation at small strain amplitudes, whereas the relaxation time of polymer chains becomes less than about a hundred oscillation periods at strain amplitudes above a few percent. By computing the peak value of the dynamical susceptibility, we estimated the dynamical correlation length that was found to exhibit a distinct maximum at the critical strain amplitude. Therefore, it was concluded that the transition from slow to fast relaxation dynamics is associated with the largest number of monomers involved in the correlated motion.

The post-processing analysis of all monomer trajectories, based on the cage decomposition algorithm [19], indicated that mobile monomers tend to aggregate into transient clusters. It was observed that the typical cluster size during intermittent bursts increases at larger strain amplitudes, which is in agreement with findings of the previous study on cyclic loading of a binary Lennard-Jones glass [21]. The effect of dynamic facilitation of mobile monomers by their neighbors becomes more pronounced with increasing strain amplitude.

In the future, it would be instructive to perform a finite-size scaling analysis of the dynamic correlation length in the vicinity of the critical strain amplitude and to explore the influence of oscillation frequency on the structural relaxation dynamics in polymer glasses.

Acknowledgments

Financial support from the National Science Foundation (Grant No. CBET-1033662) is gratefully acknowledged. Computational work in support of this research was performed at Michigan State University's High Performance Computing Facility and the Ohio Supercom-

puter Center.

-
- [1] H. E. H. Meijer and L. E. Govaert, *Prog. Polym. Sci.* **30**, 915 (2005).
 - [2] L. C. E. Struik, *Physical Aging in Amorphous Polymers and Other Materials* (Elsevier, Amsterdam, 1978).
 - [3] H. Eyring, *J. Chem. Phys.* **4**, 283 (1936).
 - [4] J.-L. Barrat and A. Lemaitre, “Heterogeneities in amorphous systems under shear,” in *Dynamical Heterogeneities in Glasses, Colloids, and Granular Media* (Oxford University Press, 2011), chap. 8.
 - [5] R. S. Hoy and M. O. Robbins, *J. Polymer Science Part B: Polymer Physics* **44**, 3487 (2006).
 - [6] C. Bennemann, C. Donati, J. Baschnagel, and S. C. Glotzer, *Nature* **399**, 246 (1999).
 - [7] Y. Gebremichael, T. B. Schroder, F. W. Starr, S. C. Glotzer, *Phys. Rev. E* **64**, 051503 (2001).
 - [8] M. Aichele, Y. Gebremichael, F. W. Starr, J. Baschnagel, S. C. Glotzer, *J. Chem. Phys.* **119**, 5290 (2003).
 - [9] A. Smessaert and J. Rottler, *Phys. Rev. E* **88**, 022314 (2013).
 - [10] L. S. Loo, R. E. Cohen, K. K. Gleason, *Science* **288**, 116 (2000).
 - [11] H.-N. Lee, K. Paeng, S. F. Swallen, M. D. Ediger, *J. Chem. Phys.* **128**, 134902 (2008).
 - [12] H.-N. Lee, K. Paeng, S. F. Swallen, M. D. Ediger, *Science* **323**, 231 (2009).
 - [13] F. M. Capaldi and M. C. Boyce, and G. C. Rutledge, *Phys. Rev. Lett.* **89**, 175505 (2002).
 - [14] A. V. Lyulin, B. Vorselaars, M. A. Mazo, N. K. Balabaev, M. A. J. Michels, *Europhys. Lett.* **71**, 618 (2005).
 - [15] G. J. Papakonstantopoulos, R. A. Riggleman, J.-L. Barrat, J. J. de Pablo, *Phys. Rev. E* **77**, 041502 (2008).
 - [16] R. A. Riggleman, H.-N. Lee, M. D. Ediger, and J. J. de Pablo, *Soft Matter* **6**, 287 (2010).
 - [17] M. Warren and J. Rottler, *Phys. Rev. Lett.* **104**, 205501 (2010).
 - [18] M. Warren and J. Rottler, *J. Chem. Phys.* **133**, 164513 (2010).
 - [19] R. Candelier, O. Dauchot, and G. Biroli, *Phys. Rev. Lett.* **102**, 088001 (2009).
 - [20] D. Fiocco, G. Foffi, S. Sastry, *Phys. Rev. E* **88**, 020301(R) (2013).
 - [21] N. V. Priezjev, *Phys. Rev. E* **87**, 052302 (2013).
 - [22] C. F. Schreck, R. S. Hoy, M. D. Shattuck, and C. S. O’Hern, arXiv:1301.7492 (2013).

- [23] D. Hudzinsky, M. A. J. Michels, A. V. Lyulin, *Macromol. Theory Simul.* **22**, 71 (2013).
- [24] I. Regev, T. Lookman, and C. Reichhardt, arXiv:1301.7479 (2013).
- [25] N. C. Keim and P. E. Arratia, arXiv:1308.6806 (2013).
- [26] K. Kremer and G. S. Grest, *J. Chem. Phys.* **92**, 5057 (1990).
- [27] R. B. Bird, C. F. Curtiss, R. C. Armstrong, and O. Hassager, *Dynamics of Polymeric Liquids*, 2nd ed. (Wiley, New York, 1987).
- [28] C. Bennemann, W. Paul, K. Binder, and B. Dunweg, *Phys. Rev. E* **57**, 843 (1998).
- [29] D. J. Evans and G. P. Morriss, *Statistical Mechanics of Nonequilibrium Liquids* (Academic Press, London, 1990).
- [30] M. P. Allen and D. J. Tildesley, *Computer Simulation of Liquids* (Clarendon, Oxford, 1987).
- [31] W. Paul and G. D. Smith, *Rep. Prog. Phys.* **67**, 1117 (2004).
- [32] P. H. Verdier, *J. Chem. Phys.* **45**, 2118 (1966).
- [33] J. Baschnagel and F. Varnik, *J. Phys.: Condens. Matter* **17**, R851 (2005).
- [34] L. Berthier and G. Biroli, *Rev. Mod. Phys.* **83**, 587 (2011).
- [35] O. Dauchot, G. Marty, and G. Biroli, *Phys. Rev. Lett.* **95**, 265701 (2005).
- [36] S. C. Glotzer, V. N. Novikov, and T. B. Schroder, *J. Chem. Phys.* **112**, 509 (2000).
- [37] M. Tsamados, *Eur. Phys. J. E* **32**, 165 (2010).
- [38] H. Mizuno and R. Yamamoto, *J. Chem. Phys.* **136**, 084505 (2012).
- [39] R. Candelier, O. Dauchot, and G. Biroli, *Europhys. Lett.* **92**, 24003 (2010).
- [40] R. Candelier, A. Widmer-Cooper, J. K. Kummerfeld, O. Dauchot, G. Biroli, P. Harrowell, and D. R. Reichman, *Phys. Rev. Lett.* **105**, 135702 (2010).
- [41] J. P. Garrahan and D. Chandler, *Proc. Natl. Acad. Sci. USA* **100**, 9710 (2003).
- [42] M. N. J. Bergroth, M. Vogel, and S. C. Glotzer, *J. Phys. Chem. B* **109**, 6748 (2005).

Figures

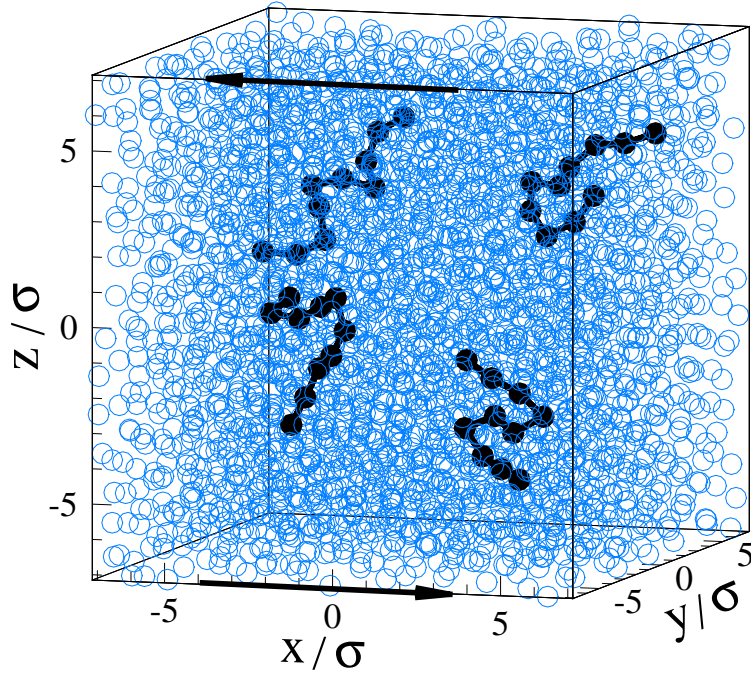


FIG. 1: (Color online) A snapshot of the polymer glass during homogeneous time-periodic shear deformation with the strain amplitude $\gamma_0 = 0.02$ and frequency $\omega\tau = 0.05$. Four chains of $N = 10$ monomers are marked by solid lines and filled circles (not drawn to scale). The black arrows indicate the direction of the applied shear strain. The Lees-Edwards periodic boundary conditions are imposed in the xz plane.

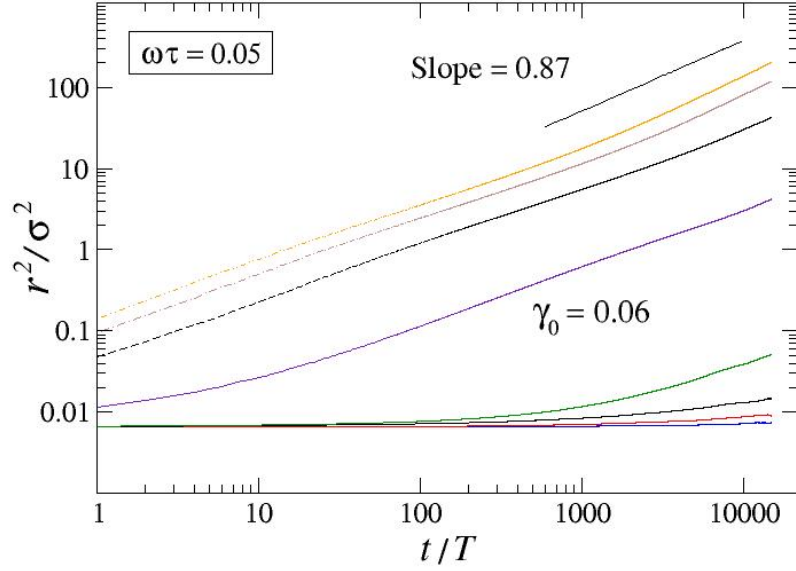


FIG. 2: (Color online) The averaged mean-square displacement of monomers as a function of time for the oscillation frequency $\omega\tau = 0.05$ and period $T = 2\pi/\omega = 125.66\tau$. The strain amplitudes from bottom to top are $\gamma_0 = 0.02, 0.03, 0.04, 0.05, 0.06, 0.07, 0.08,$ and 0.09 . The straight black line with the slope 0.87 is shown for reference.

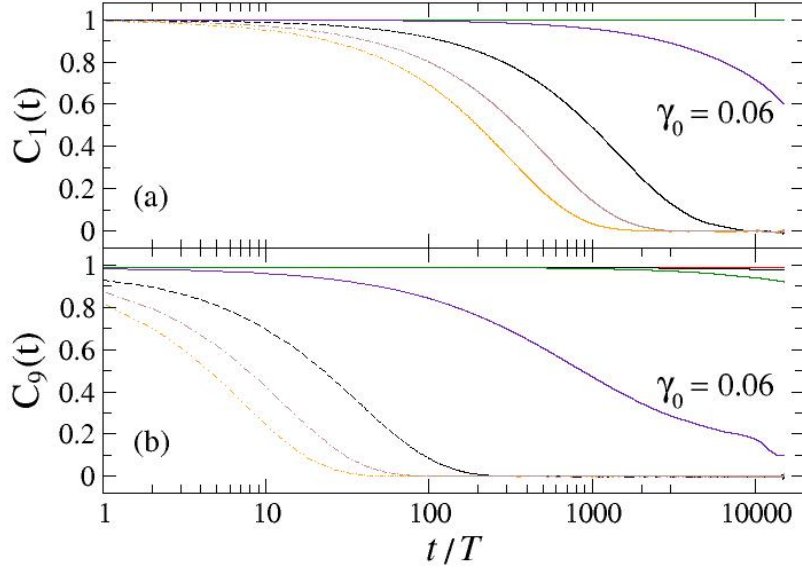


FIG. 3: (Color online) The autocorrelation function of (a) $p = 1$ and (b) $p = 9$ normal modes defined by Eq. (5) for the oscillation frequency $\omega\tau = 0.05$ and period $T = 2\pi/\omega = 125.66\tau$. The strain amplitudes from top to bottom are $\gamma_0 = 0.02, 0.03, 0.04, 0.05, 0.06, 0.07, 0.08,$ and 0.09 .

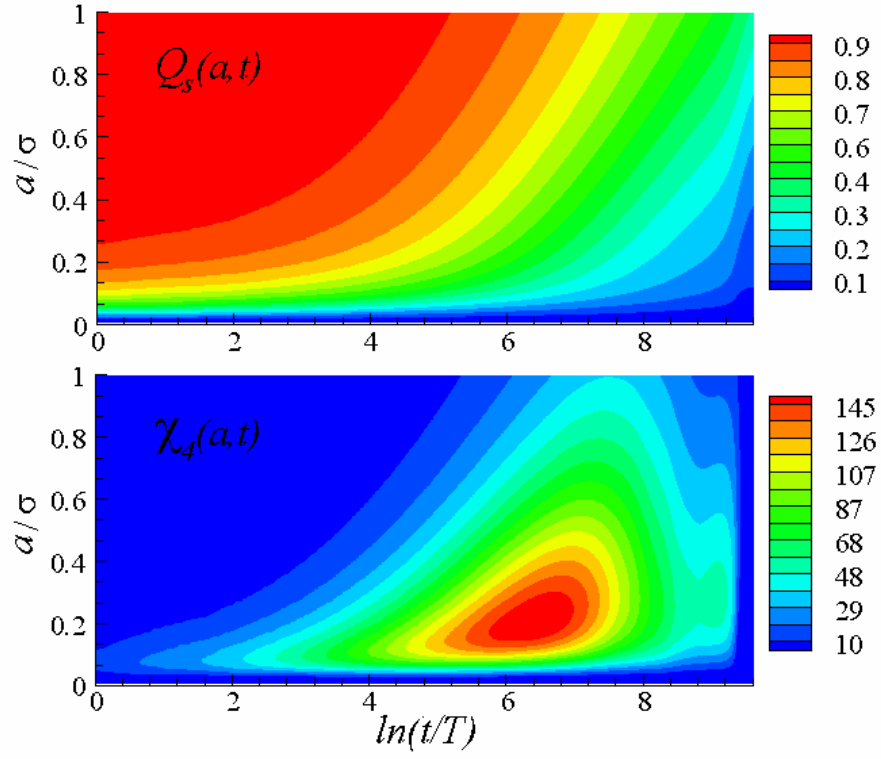


FIG. 4: (Color online) The contour plots of the correlation functions $Q_s(a, t)$ (top) and $\chi_4(a, t)$ (bottom) for the strain amplitude $\gamma_0 = 0.06$ and oscillation frequency $\omega\tau = 0.05$. The oscillation period is $T = 125.66\tau$.

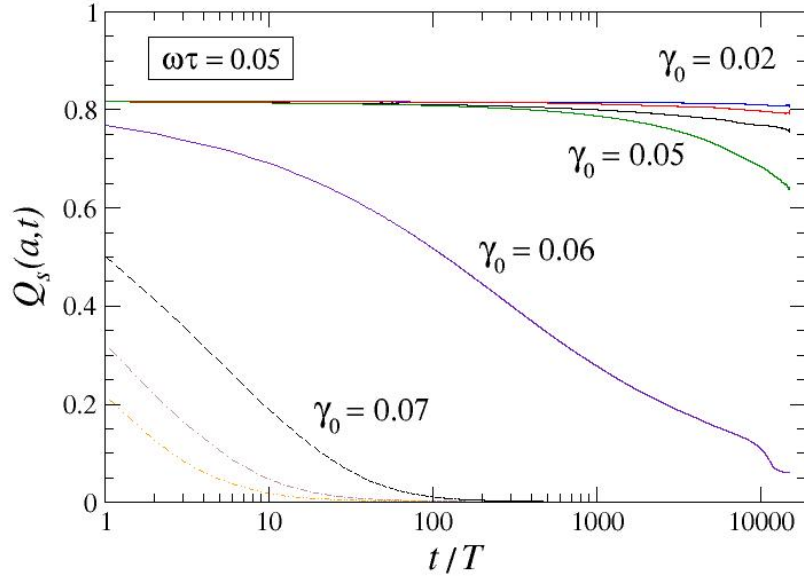


FIG. 5: (Color online) The time dependence of the self-correlation function $Q_s(a, t)$ computed at $a = 0.12\sigma$ for the oscillation frequency $\omega\tau = 0.05$ and period $T = 2\pi/\omega = 125.66\tau$. The strain amplitudes from top to bottom are $\gamma_0 = 0.02, 0.03, 0.04, 0.05, 0.06, 0.07, 0.08,$ and 0.09 .

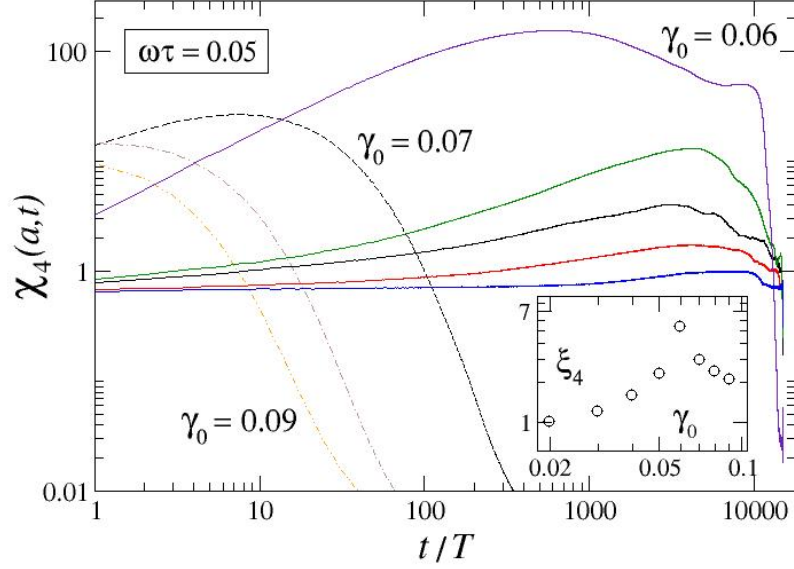


FIG. 6: (Color online) The dynamic susceptibility $\chi_4(a, t)$ defined by Eq. (7) for the oscillation frequency $\omega\tau = 0.05$ and period $T = 2\pi/\omega = 125.66\tau$. The strain amplitudes from bottom to top are $\gamma_0 = 0.02$ at $a = 0.06\sigma$, $\gamma_0 = 0.03$ at $a = 0.06\sigma$, $\gamma_0 = 0.04$ at $a = 0.07\sigma$, $\gamma_0 = 0.05$ at $a = 0.08\sigma$, $\gamma_0 = 0.06$ at $a = 0.21\sigma$. The other curves correspond to $\gamma_0 = 0.07$ at $a = 0.20\sigma$ (dashed curve), $\gamma_0 = 0.08$ at $a = 0.17\sigma$ (dash-dotted curve), and $\gamma_0 = 0.09$ at $a = 0.19\sigma$ (dash-double-dotted curve). The inset shows the dynamic correlation length $\xi_4 = [\chi_4^{\max}(a, t)]^{1/3}$ as a function of the strain amplitude γ_0 .

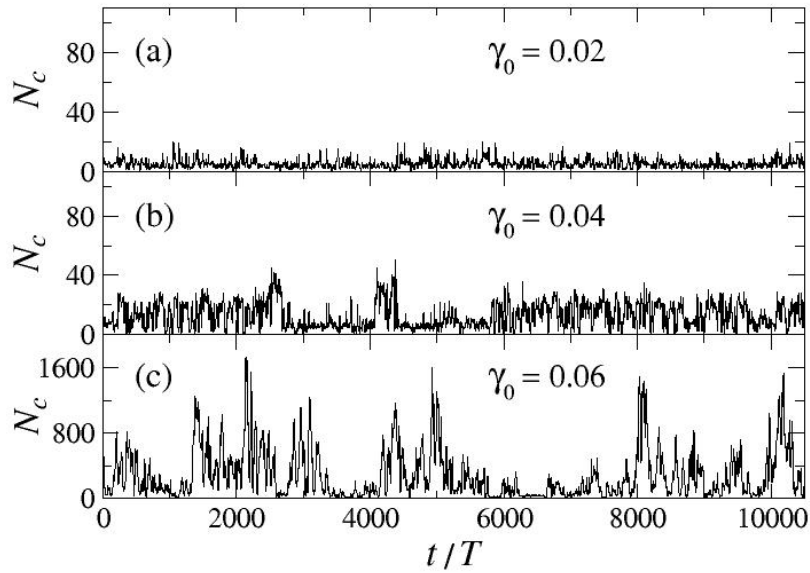


FIG. 7: (Color online) The total number of mobile monomers during cyclic deformation with frequency $\omega\tau = 0.05$, period $T = 2\pi/\omega = 125.66\tau$, and strain amplitudes (a) $\gamma_0 = 0.02$, (b) $\gamma_0 = 0.04$, and (c) $\gamma_0 = 0.06$.

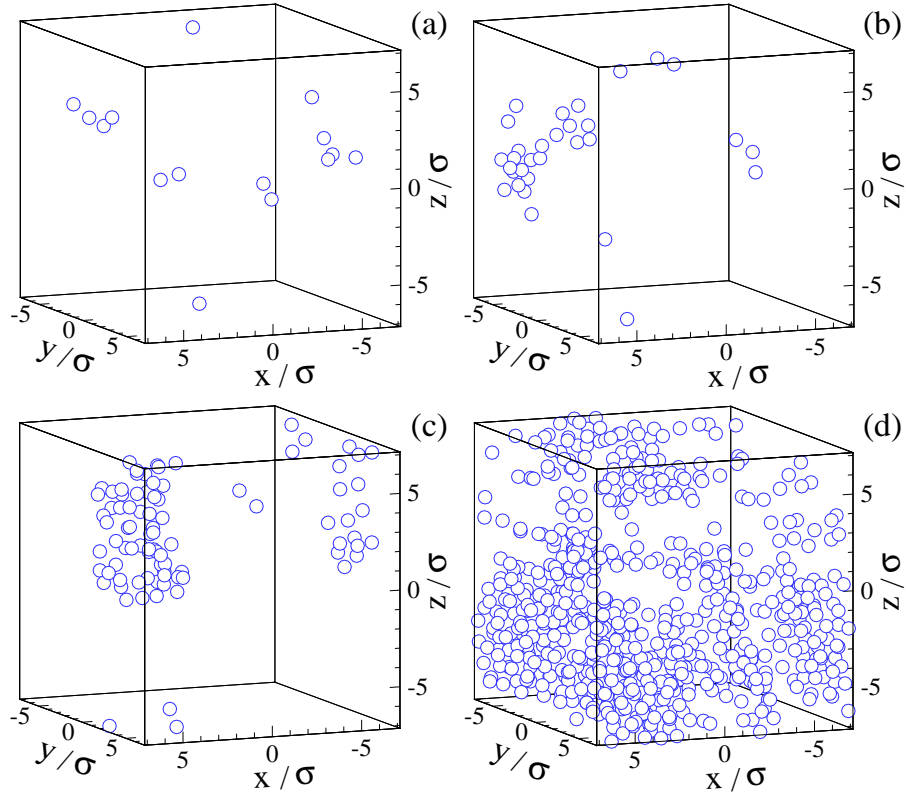


FIG. 8: (Color online) Snapshots of mobile monomer configurations at strain amplitudes (a) $\gamma_0 = 0.03$, (b) $\gamma_0 = 0.04$, (c) $\gamma_0 = 0.05$, and (d) $\gamma_0 = 0.06$.

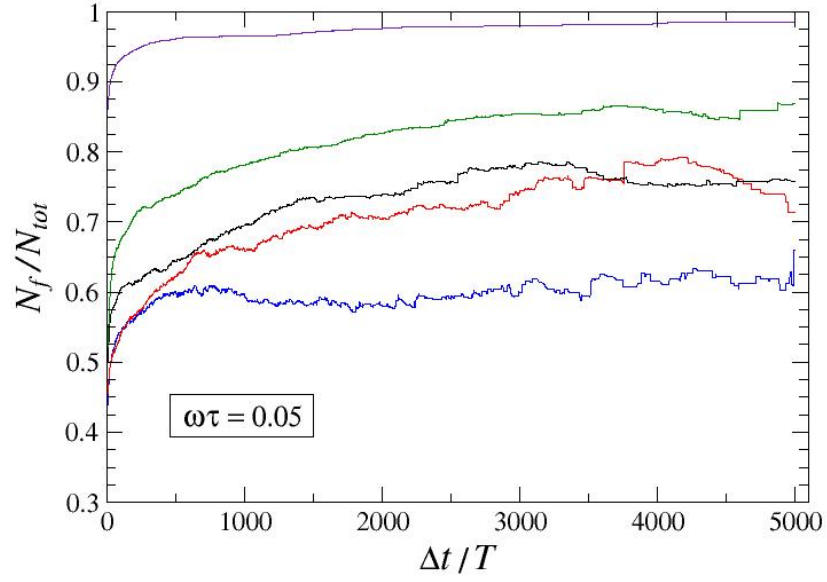


FIG. 9: (Color online) The ratio of dynamically facilitated mobile monomers and the total number of mobile monomers as a function of the time interval preceding cage jumps. The oscillation frequency is $\omega\tau = 0.05$ and strain amplitudes are $\gamma_0 = 0.02, 0.03, 0.04, 0.05,$ and 0.06 (from bottom to top).